JAAS

Laser ablation of 'diamonds-in-water' for trace element and isotopic composition analysis

Journal:	*Journal of Analytical Atomic Spectrometry*
Manuscript ID	JA-TEC-03-2022-000088.R1
Article Type:	Technical Note
Date Submitted by the Author:	25-May-2022
Complete List of Authors:	Weiss, Yaakov; Hebrew University of Jerusalem, Jockusch, Steffen; Bowling Green State University, Chemistry Koornneef, Janne; Vrije Universiteit Amsterdam, Earth Science Department Elazar, Oded; Hebrew University of Jerusalem Davies, Gareth; Vrije Universiteit Amsterdam, Geology & Geochemistry

TECHNICAL NOTE

Laser ablation of 'diamonds-in-water' for trace element and isotopic composition analysis

Received 00th January 20xx,
Accepted 00th January 20xx

DOI: 10.1039/x0xx00000x

Yaakov Weiss,*[a,b] Steffen Jockusch,[c,d] Janne M. Koornneef,[e] Oded Elazar[a] and Gareth R. Davies[e]

A new laser ablation technique combined with mass spectrometry measurements was applied for trace elements and radiogenic isotopic analyses of high-density fluid (HDF) microinclusion-bearing diamonds. Experiments were conducted using a frequency-doubled Nd:YAG laser (532 nm, 150 mJ/pulse, 7 ns pulse duration, 30 Hz repetition rate) in a closed ultra-clean glass cuvette filled with ultrapure water. Five diamonds were ablated for 1 hour while a single diamond was repeatedly ablated for shorter periods to produce 4 different weights of ablated material. Ablations proceeded at an average rate of 7.8 mg/h, which is a factor of >10 better than previous studies. ICPMS trace element analyses of the ablated material reveal primitive mantle normalized patterns that are similar in shape to previously analyzed microinclusion-bearing diamonds. Importantly, the new ablation technique produces enough material for quantitative analysis of all rare-earth elements (REEs), even in diamonds of low element abundance levels. The 4 duplicates of a single diamond were analyzed for their Sr, Nd, and Pb isotope compositions by TIMS using 10^{11} or 10^{13} Ω resistors. The results reveal a relationship between decreasing amounts of analyte and increasing Sr and Pb isotope ratios attributed to blank contribution. No blank influence is detected on Nd isotope ratios. Ablations of a few mg provide sufficient amount of analyte to yield comparable Sr-Nd-Pb isotope values that reflect the composition of the ablated diamond. This result also suggests that HDF microinclusions within individual diamonds are rather homogeneous in their isotopic composition.

Introduction

High-density fluid (HDF) microinclusions in diamonds provide a direct sample of carbon- and water-rich fluids in the Earth's mantle. The study of such HDFs provides unique information on the origin of natural diamonds and offers the potential to determine the range of compositions of deep-Earth volatile-rich media, their varying mantle sources, and the possible changes in their nature through geological time [e.g. 1-6].

The trapped HDF material amounts to <1% of the diamond by weight, so major elements such as Si or Mg are present only at trace levels even in zones that are highly populated with microinclusions [7]. The analysis of these sub-micrometer inclusions poses analytical challenges. Nonetheless, over 30 years of studies of ~300 microinclusion-bearing diamonds by electron probe micro-analyzer (EPMA) and infra-red (IR) spectroscopy revealed that HDFs vary in composition between four types: high- and low-Mg carbonatitic, hydrous-silicic and hydrous-saline compositions [e.g. 8-15].

The concentrations of Ba, Rb, Sr and some rare-earth elements (REEs) in a microinclusion-bearing diamond from an unknown source were first determined by Bibby (1979) [16] using instrumental neutron activation analyses (INAA). These elements and Sr isotope compositions were also measured in 5 microinclusion-bearing diamonds from the Democratic Republic of the Congo (DRC) by Akagi and Masuda (1988) [17], who burnt the diamonds and analyzed the residue using isotope dilution mass spectrometry. Additional trace elements and some major elements (including K, Na, Fe Zr, Cs, Hf, Ta, Th and U) were measured in a suite of diamonds from Jwaneng, Botswana, by Schrauder et al. (1996) [5] using INAA. However, the development of laser ablation inductively coupled plasma mass spectrometry (LA-ICPMS), allowed fast and easy measurement of many trace elements in microinclusion-bearing diamonds [e.g. 11, 15, 18-22]. Such data led Weiss et al. (2013) [23] to distinguish between two principle trace-element patterns in HDFs, one with high field strength element (HFSE) depletions and large ion lithophile element (LILE) enrichments (similar to calc-alkaline magmas and continental rocks) and the other with lower LILE abundances and 'smoother' overall trace element patterns (similar to oceanic basalts).

In an attempt to analyze trace elements concentrations in gem-quality diamonds, barren of visible microinclusions aggregates, an 'off-line' laser ablation approach was developed that allows increase of the analyte levels for ICPMS analyses [24, 25]. The technique was also applied to microinclusion-bearing diamonds producing trace element results comparable to previous analyzes of the same diamonds [26]. More importantly,

[a] The Freddy and Nadine Herrmann Institute of Earth Sciences, The Hebrew University of Jerusalem, Jerusalem 91904, Israel. *yakov.weiss@mail.huji.ac.il
[b] Lamont-Doherty Earth Observatory of Columbia University, Palisades, New York 10964, USA
[c] Department of Chemistry, Columbia University, New York, New York 10027, United States
[d] Center for Photochemical Sciences, Bowling Green State University, Bowling Green, Ohio 43403, United States
[e] Vrije Universiteit Amsterdam, Faculty of Earth and Life Sciences, De Boelelaan 1085, 1081 HV Amsterdam, The Netherlands

it provided a new opportunity for radiogenic isotopic analyses of such diamonds [26, 27], more than two decades after the first and only Sr isotope data of 5 DRC diamonds that were published previously by Akagi and Masuda [17]. To date, 42 microinclusion-bearing diamonds from Canada, Botswana, DRC, Guinea, and Siberia were analyzed for their Sr isotope compositions using this off-line laser ablation and MS analyses method [1, 26-28]. In comparison radiogenic isotopic data for Nd and Pb are very scarce, only five microinclusion-bearing diamonds were analyzed for their Nd and only three for their Pb isotope compositions. The main reason is that only diamonds with high total trace element abundances could be analyzed [26, 27]. Therefore, the determination of Sr-Nd-Pb isotope compositions of microinclusion-bearing diamonds remains challenging.

Here we assess the viability of an off-line ablation technique of diamonds-in-water using a 'powerful laser' to significantly improve the amount of ablated material. We show that the method significantly improves the analyses of heavy rare-earth elements (HREEs), which could not be quantitatively determined in previous studies. Moreover, we demonstrate that the amount of collected analyte combined with recent advances in TIMS technology, i.e. the use of 10^{13} Ω resistors that allow isotope analysis of exceedingly low abundances [29], facilitate Sr-Nd-Pb isotope analyses of such diamonds. We discuss the impact of the ablated material weight on the precision of the results and the compositional variation within an individual microinclusion-bearing diamond.

Experimental

Diamond samples

Six microinclusion-bearing diamonds from a single source in Canada (exact origin unknown) were selected, processed, and analyzed for the present study. The diamonds are all 3 to 4 mm in diameter, vary in weight between 91 to 116 mg, have cubic morphology, and are light- to dark grey in color (Fig. 1). Each diamond was laser-cut twice to create two parallel side sections and a central thin plate, that was polished on both sides using a cast-iron diamond-polishing wheel. EPMA analyses at the Hebrew University of Jerusalem were used for determining the major element composition of the microinclusions, which range between silicic to low-Mg carbonatitic HDFs. No systematic radial (core-to-rim) compositional change was observed for any of the diamonds (Fig. 2), and the major and minor oxides of the individual HDF microinclusions span a range that varies by 7-23% (1σ) for SiO_2, 8-21% for K_2O, 14-34% for Al_2O_3, MgO, FeO, CaO, Na_2O, 23-35% for P_2O_5 and 24-44% for Cl. Such diamonds are considered homogeneous for their major element HDF compositions [7].

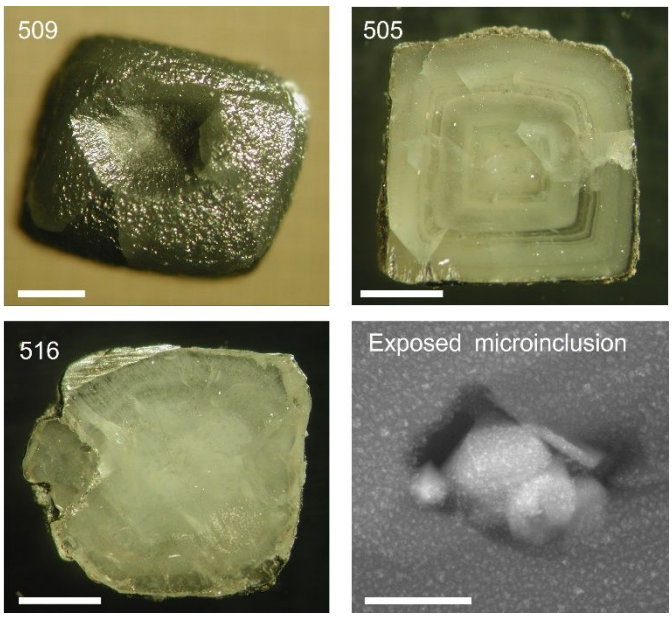

Fig. 1 Images of selected microinclusion-bearing diamonds used for the present study and an exposed microinclusion. Diamonds 509 - before cutting and polishing; 505 and 516 - double-sided polished plates. Some diamonds formed as duo cube aggregates, as seen in diamond 516; the smaller crystal has become dislodged in diamond 509. The high-resolution SEM image of the microinclusion show a multi-phase assemblage of secondary minerals (carbonates, silicates and phosphates) that grew from the HDF upon cooling of the diamond; the vacancy was occupied by residual low-density hydrous solution and possibly other daughter phases that were lost during cleaving [11, 30-32]. The scale bar is 1 mm in all diamond panels and 500 nm for the microinclusion.

Analytical methods

We present a new off-line laser ablation technique of diamonds that allows analysis of analyte collected from a few mg of ablated material for trace element and isotopic composition. The laser ablation procedure was developed and performed at Lamont-Doherty Earth Observatory (LDEO) and the Department of Chemistry of Columbia University. Sample preparation, post-ablation processing and digestion in PicoTrace Ultra-Clean laboratory and trace element analysis were carried out at LDEO. Element separation by ion-exchange column chromatography and isotope analysis were performed at the Vrije Universiteit Amsterdam (VU).

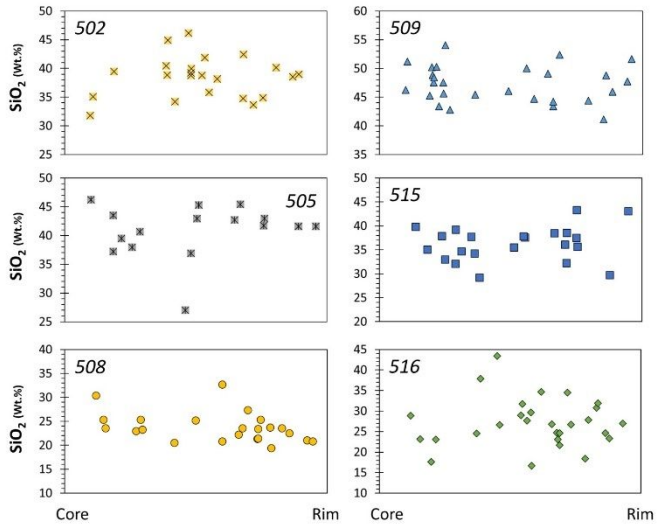

Fig. 2 The SiO_2 (in wt.%) content of the microinclusions vs. their position between the core and the rim in the studied diamonds. Precision is approximately 2σ(%)=2/oxide in wt.% [33], and is <2% for SiO_2 in the analyzed microinclusions. The compositional range of individual microinclusions in a single diamond span a range that reflects variation in the chemistry of the trapped HDFs; no systematic radial changes were observed and such diamonds are considered homogeneous for their microinclusions composition [7].

Sample preparation, ablation, and processing

The ablation method follows the off-line concept of ablation in a closed-system cell that is not connected to a mass spectrometer, followed by solution trace elements and isotopic analyses of the produced analyte [24, 27]. Previous off-line ablation studies utilized low power lasers for on-line ablation and geological applications (i.e. 213 nm Nd:YAG and 193 nm ArF Excimer lasers [e.g. 26, 34]). In contrast, we used a Nd:YAG laser (532 nm, 150 mJ/pulse, 7 ns pulse duration, 30 Hz repetition rate) that allows high diamond ablation rate. In addition, we performed the ablation while the diamond is completely submerged in water to improve recovery efficiency (Fig. 3a,b).

Laser ablation of solids in liquid is widely used for industrial fabrication of nano-particles in many materials [35-39], and was explored as a possible sampling technique for analysis of standard reference materials (i.e. NIST 610 and 611 [40, 41]). However, to our knowledge, such an ablation technique was never used for processing and chemical analyses of natural geological samples. The combination of a powerful laser and ablation in water for the study of trace elements and isotopic compositions of microinclusion-bearing diamonds has two major advantages. First, the amount of diamond that can be ablated using such a laser is several mg/h (Table 1). Second, the trapping efficiency by ablation in water is very high and allows retrieval of >98% of the nanosized analyte particles [42]. In addition, the entire trapped microinclusions are ablated and digested by acids, so possible elemental and isotopic fractionation induced by ablation are avoided.

We used a custom-modified quartz Fluorometer cell (3-Q-20, 7.0 ml, Starna Cells) as an ablation cell. Diamonds and milli-Q water (milli-Q, 18.2 MΩ cm) can be placed in the cell and sealed in an ultra-clean environment. The Fluorometer cell was cleaned in 8N double-distilled (DD) HNO_3 for a minimum of 7 days and PTFE parts were cleaned in 16N DD HNO_3 at 180 °C for 4 hours before they were stored in 8N DD HNO_3; all parts were rinsed in milli-Q water before use. Each diamond was cleaned in a mixture of 16N DD HNO_3 and 29N DD HF on a hotplate at 120 °C for several hours, then rinsed in milli-Q water and mounted by a tailored PTFE ring into the PTFE holder (+lid), before it was placed in the cell and milli-Q water was added (4 ml; Fig. 3b). Diamond-in-water ablation was performed using a Spectra-Physics GCR-150-30 Q-switched Nd:YAG laser. The fundamental laser output light of 1064 nm was frequency-doubled to generate a beam of 532 nm with a power of ~150 mJ/pulse, 7 ns pulse duration, diameter of 8 mm and operated at 30 Hz. The laser beam was spot-focused on the diamond using an aspheric condenser lens (25 mm focal length; Fig. 3a,b).

Each diamond was weighed 3 times using a Mettler Toledo XP6 microbalance, before and after ablation, to determining the weight of the ablated material with a precision of ±1 µg. The offcut side section of 5 of the diamonds were ablated for 60 minutes. One diamond (509) was ablated repeatedly for ~1, 5, and twice for 30 minutes, to produce 4 duplicates of different weights of ablated material. We use these duplicates to evaluate the reproducibility of the new diamond-in-water ablation method and the effect of varying analyte weight on the analytical results. In addition, the results of the 4 duplicates permit the assessment of trace elements and isotopic compositional variation within an individual diamond.

Following ablation, the cell was opened in an ultra-clean chemistry environment and the ablated material solution was transferred to a clean PFA beaker. An additional 1 ml of milli-Q water was used to wash the ablation cell and transferred to the beaker, before drying down at 80 °C. The sample was then digested using a 1.2 ml mixture (5:1) of 16N DD HNO_3 and 29N DD HF at 120 °C, dried down again at 80 °C and re-dissolved in 1 ml of 1N DD HNO_3 before analyses. An aliquot of 200 µl of each sample was separated for trace elements analyses whereas the remaining 800 µl was processed for Sr-Nd-Pb isotope measurements.

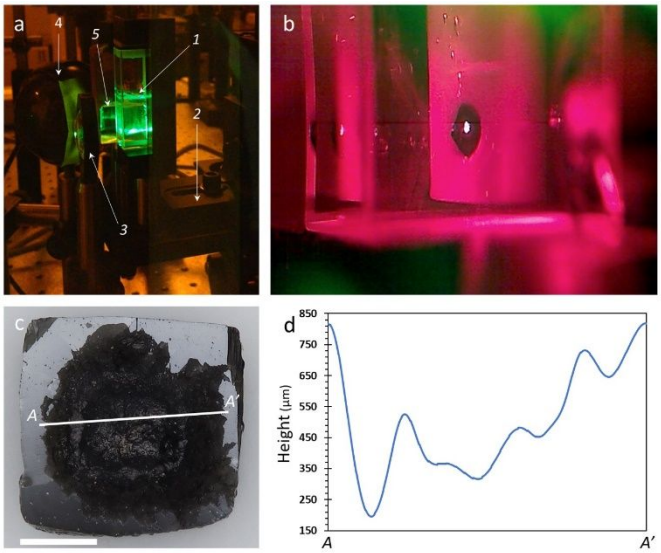

Fig. 3 Ablation of diamond-in-water and process outcome. **(a)** The system setup includes the ablation cell *(1)* that is mounted onto a manual micrometer stage *(2)*, an aspheric condenser lens *(3)* that focuses the laser beam on the diamond, a web camera *(4)* connected to a computer, and an optical prism with a 570 nm long-pass filter *(5)* that allows a clear view into the cell during ablation. The level of milli-Q water in the cell is about ½ of its volume. The laser source is to the left and outside the frame of the photograph, but its course through the water in the cell is seen. **(b)** A close-up snapshot of the cell taken during diamond ablation; the cuboid diamond (dark) is mounted into the PTFE holder (bright pink) using a tailored PTFE ring and is completely submerged in milli-Q water. Bubbles are seen rising from the ablated surface of the diamond (bright spot in the center of the diamond). Photo was taken through the optical prism+filter to eliminate the green laser radiation. **(c)** Photomicrograph of diamond 505 after ablation; scale bar is 1 mm. **(d)** A cross-section profile along A-A' in (c) showing the vertical depth variation within the ablation pit (measured using the 3D model function of a Hirox HR-2000 optical microscope).

Trace element analysis

Trace element concentrations of all diamonds were determined using a VG PlasmaQuad ExCell quadrupole ICPMS. The samples were diluted to 1 ml using 3% DD HNO_3. Solutions were introduced to the ICPMS with a desolvation system (CETAC Aridus), which enhances sensitivity and reduces solvent-based interferences (i.e. oxides and hydrides). The instrument was operated in a pulse counting mode, under plasma conditions of 1350 W Radio Frequency (RF) power and 13 l/min of cool gas flow. The oxide formation rate (<1% for Ce) was checked by using a 100 ng/L Ce tune solution and sensitivity was optimized before analyses. We determined the solution concentrations against 6 point calibration lines of an in-house multi-element standard, spanning the expected concentration range of our samples, and an internal standard of 1 ppb In. All concentrations were corrected for instrumental drift, and for the average total procedural blank values. Errors in trace element concentrations are estimated at ~2%, based on the laboratory multiple runs of a calibration curve from repeated measurements of in-house multi-element solutions and rock standards.

Chromatography and Isotopic analysis

Chemical separation of Sr, Nd and Pb from a single solution of each of the dissolved duplicates of diamond 509 was performed using miniaturized chromatographic separation procedures developed for ultra-low blank contributions. The column yields are ~97 % for Pb, >95 % for Sr and >90 % for Nd and small aliquots of international reference materials (AGV-1 and BHVO-2) give accurate results [29, 43, 44]. Isotope compositions were measured by TIMS using a Thermo Scientific TRITON Plus instrument equipped with 10^{11} and 10^{13} Ω resistors. All clean lab protocols and procedures, and instrumental measuring routines and cup configuration were fully outlined in [29, 45, 46]; here, only a summary is given.

Pb was separated first. Columns were loaded with pre-cleaned AG 1-X8 200–400 mesh resin and washed three times with alternating 6N HCl, 2M HF, and milli-Q water before conditioning with 0.7M HBr. The full samples dissolved in 0.5 ml 0.7M HBr were then loaded onto the columns. Subsequently, the matrix was rinsed with 1 ml 0.7M HBr followed by 0.15 ml 3.0M HCl and eluted with 0.6 ml 6.5M HCl. The resin is discarded after use. The collected Pb fractions were divided by weight to 'natural' and 'spiked' fractions (~66.6% and 33.3%, respectively), the latter was double spiked using an in-house VU_^{207}Pb-^{204}Pb mix standard with a ratio of 0.79086±7 calibrated against standard reference material NIST SRM 982 [47]. Pb isotope ratios of international standards that were previously processed using this protocol are within analytical error of the accepted values [44, 45]; demonstrating that possible mass-induced fractionation of Pb isotopes by column chromatography is insignificant. Both fractions were dried down and nitrated twice with 2 drops of concentrated HNO_3 to eliminate organic material. The dried samples were re-dissolved in 2 µl 10% HNO_3 before they were loaded on outgassed zone-refined rhenium filaments. First, 1.5 µl of silica gel was loaded to which the sample in 2 µl was added drop by drop. The solution was evaporated at 1.0 A and fused at 2.0 A. Spiked Pb fractions were dried down and loaded similarly to the natural sample fractions. The natural sample fractions were analyzed using a 10^{13} Ω resistor for the detection of ^{204}Pb in combination with regular 10^{11} Ω resistors for the other isotopes; all were run to exhaustion. Spiked fractions were analyzed using 10^{11} Ω resistors. As the double spike inversion cannot be solved algebraically, it was processed individually per sample in an offline spreadsheet. Both natural and spiked data were subjected to an artificial mass fractionation correction that allows a realistic estimate of the analytical uncertainties. The corrected data were subjected to a 2σ outlier test, algebraic error propagation, and instrumental mass fractionation correction. Uncertainties were propagated algebraically and take into account the strong error correlation (r > 0.90) between ^{20x}Pb/^{204}Pb ratios. Instrumental reproducibility during analyses was monitored using an NBS981 standard 40 ng that gave average values of ^{206}Pb/^{204}Pb=16.9414 ± 7, ^{207}Pb/^{204}Pb=15.4990 ± 10 and ^{208}Pb/^{204}Pb=36.7257 ± 12. A single load of NBS981 2 ng

gave $^{206}Pb/^{204}Pb$=16.9350 ± 46, $^{207}Pb/^{204}Pb$=15.4933 ± 40 and $^{208}Pb/^{204}Pb$=36.712 ± 10, and NBS981 200 pg gave $^{206}Pb/^{204}Pb$=16.9383 ± 18, $^{207}Pb/^{204}Pb$=15.5097 ± 16 and $^{208}Pb/^{204}Pb$=36.719 ± 38. An aliquot solution of BHVO-2 containing ~130 pg was processed along with the individual sample batches to monitor and ensure data quality; it gave $^{206}Pb/^{204}Pb$=18.55 ± 21, $^{207}Pb/^{204}Pb$=15.502 ± 20 and $^{208}Pb/^{204}Pb$=38.089 ± 58. The small variation from the Georem values (18.647 ± 24, 15.533 ± 9 and 38.237 ± 18 [48]) could result from the small amount that was processed in the present study and a blank contribution or be assigned to the BHVO-2 powder not being homogeneous for Pb as it was processed using a tungsten carbide crushing method.

Sr and REEs were simultaneously separated by placing the Sr column above the TRU column each containing pre-cleaned resins. Sample solutions were spiked with ^{84}Sr and a ^{149}Sm-^{150}Nd mixed spike aiming for a sample/spike ratio of 20-100 for Sr and 20 for Nd (before Pb columns separation). The columns were cleaned with 1 reservoir each of 3M HNO_3, 2M HF, 3M HNO_3, 1M HF, milli-Q, 3M HNO_3, 1M HF and milli-Q before conditioning with half a reservoir 3M HNO_3. The samples were then loaded onto the Sr columns and washed with 0.3 ml 3M HNO_3, so the fraction from the Sr column was directly eluted onto the TRU column, after which the two-column sets were separated. The Sr columns were washed with 0.75 ml 3M HNO_3 before Sr was eluted with 0.5 ml milli-Q, and the TRU columns included 1 ml 2M HNO_3 and 2.25 ml 2M HNO_3 before elution of the REE with 1.5 mL milli-Q. Sr and TRU resin is discarded after use. Subsequently, the REE fraction was dried down and taken up in 1 ml 0.165M HCl before Nd separation using Ln-columns. These columns were pre-cleaned with 1 reservoir each of 6M HCl, 2M HF, milli-Q and 6-7M HCl before conditioning with 0.165M HCl. Upon sample loading, the columns were washed with 3 ml 0.165M HCl. Nd was then collected with 1.6 mL 0.3M HCl. The Sr and Nd fractions were dried down and re-dissolved in 3 µl 10% HNO_3 before they were loaded on pre-cleaned outgassed rhenium filaments. First, 1.5 µl of a solution containing $TaCl_5$ (100ng/µL) was loaded as an activator for Sr while 1.5 µl 10% H_3PO_4 was used to control ionization for Nd, to which the sample in 3 µl was added drop by drop. The solution was evaporated at 1.0 A and fused at 2.0 A. All Sr samples and two samples with >5 ng Nd (509C,D, preliminary indicated by ICP-MS analyses) were measured on Faraday cups with 10^{11} Ω resistors, whereas the remaining Nd samples were analyzed using a 10^{13} Ω resistors. Most samples were run to exhaustion. The Sr and Nd isotope data are normalized for mass fractionation in the mass spectrometer to overcome any mass fractionation induced by chromatography or mass spectrometry. NBS987 standard of 200, 10, 5, and 1 ng Sr gave an average value of $^{87}Sr/^{86}Sr$=0.710254 ± 13; JNDi-1 standard of 200 ng Nd gave an average $^{143}Nd/^{144}Nd$=0.512111 ± 44 and an in-house CIGO 2ng and 200 pg standards gave an average $^{143}Nd/^{144}Nd$=0.511335 ± 46. BHVO-2 aliquots containing ~35.5 and 3.6 ng Sr and ~2.2 ng and 220 pg Nd, respectively, gave an average $^{87}Sr/^{86}Sr$=0.703538 ± 39 and $^{143}Nd/^{144}Nd$=0.513073 ± 141; in agreement with its reference values 0.703479 ± 20 and 0.512984 ± 11 [48].

Total procedural blanks

Our total procedural blank (TPB) incorporates all aspects of the new diamond-in-water ablation method (except for ablation itself), including cleaning and preparation of ablation cells and samples, associated ablation practices, post-ablation protocols and chemicals, and instrumental procedures. We collected two TPBs that were treated as samples - 200 µl was used for trace elements analyses whereas the remaining 800 µl was processed for isotopic analyses.

For trace element analyses, we utilize the definition of the limit of quantification (LOQ) as 10 times the uncertainty on the blank/background (that is LOQ=10×$\sigma_{(TPB)}$ [49]), similar to previous diamond-ablation studies [e.g. 19, 24]. We consider any measurement above the LOQ as quantitative, whereas values between LOQ and the limit of detection (LOD=3×$\sigma_{(TPB)}$, Currie, 1968) are regarded as qualitative and are highlighted as such in both tables and figures. The uncertainty for the two TPBs collected is calculated as $\sigma = |x_{(TPB1)} - x_{(TPB2)}|/\sqrt{2}$ and the LOQ in ppb for the different trace elements measured by ICPMS is presented in Table 1. These are equivalent to 2-7×10^{-4} ng in 1 ml of TPB solution for Cs, Eu, Tb, Ho, Er, Tm and Lu, 1.5-5.5×10^{-3} ng for U, Pr, Sm, Gd, Dy and Yb, 1.3-4.3×10^{-2} ng for Nd, Hf and Y, 0.1-0.4 ng for Rb, Th, Nb, La and Sr, and in the range of 1.3-2.8 ng for Ba, Ce, Zr and 60 ng for Ti.

To evaluate the contribution of the TPB on the isotopic composition of the measured samples, we determined its Sr, Nd and Pb contents by isotope dilution TIMS analyses (Table 2). The two TPBs yielded 373 and 382 pg of Sr that make up <5% by weight of samples 509C,D, and 17% and 39% of the two <1 mg ablation duplicates 509A,B; and Nd of 4.8 and 7.9 pg that make up between 0.04-2.12% of the samples. The levels of Pb are higher, 225 and 239 pg in the two TPBs measured and constitute on average between 7-41% by weight of the four samples. TPBs were too small for the determination of isotopic compositions.

Results and discussion

Ablation weight and efficiency

The weight of the ablated material of the studied diamonds using the new off-line ablation technique varied between 4.9 to 14.4 mg (Fig. 4; Table 1); excluding diamond 509 that was ablated for shorter periods, producing 0.1, 0.3, 2.8 and 3.4 mg of ablated material. The ablation rate varied between 3 to 14.4 mg/h for the studied diamonds. The variation in ablation rate between different samples is mainly due to the system stage speed and incremental movement in the X-Y-Z direction, which was controlled manually during operation. This factor also influenced the ablation pit morphology and spatial depth, which are irregular and vary between ablations (Fig. 3c,d). Nonetheless, it does not affect the chemical analyses or the ability to determine the trace element and isotopic composition of the diamond+microinclusions, which is solely influenced by the amount of analyte collected.

The ablation rates are significantly higher compared to previous off-line ablations of ~250 diamonds; which demonstrated a range of ablated material between 0.01 to 2.9

mg with an average of 0.36 ± 0.29 mg, and an ablation rate between 0.007 to 0.58 mg/h with an average of 0.12 ± 0.09 mg/h (Fig. 4). The new off-line ablation technique using a powerful laser thus provides a means to increase the volume of diamond that can be ablated (relatively fast) and the amount of analyte that can be collected and analyzed.

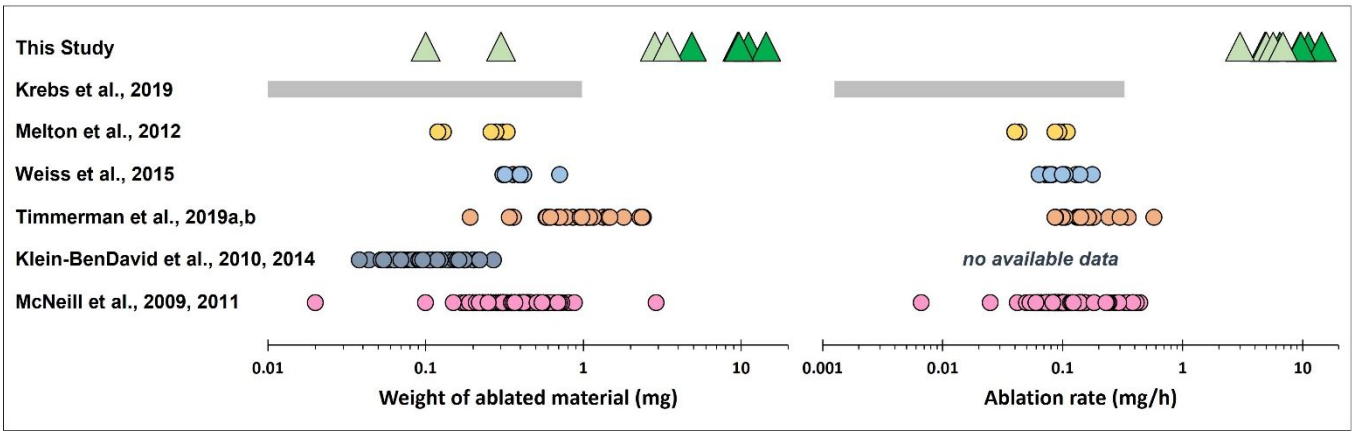

Fig. 4 Off-line diamond ablation yield and rate. The weight of ablated material (mg) and ablation rate (mg/h) of the studied diamonds using the new off-line ablation technique (green triangle data-points; the repeated ablations of diamond 509 are in light green). For comparison, all available data for previous off-line laser ablations of diamonds are presented [24-28, 34, 50-52]. Data for Krebs et al. [34] are presented as a continuous bar as only minimum and maximum weights and duration of ablation were published; the weight of ablated diamonds in Klein-BenDavid et al. [26, 27] is provided via personal communication, no data for the duration of ablations and thus ablation rates are unavailable.

Trace elements composition

The trace element compositions of the studied diamonds are mostly comparable. Primitive mantle (PM) normalized patterns show an overall decreasing levels from the most incompatible to more compatible elements with characteristic element anomalies of microinclusion-bearing diamonds [23] (Figure 5a,b). Their fractionated REEs exhibit La/Sm_{PM}, La/Dy_{PM} and La/Lu_{PM} between 8-55, 30-185 and 63-520, respectively. Cs, Rb, and Ti are relatively low compared to elements of similar compatibility and Nb, Sr and Zr (and Hf) show varying contents, mainly relative depletion but enrichment in a minority of cases. La/Nb_{PM} in four diamonds vary between 5-47 while in two diamonds it is ~1, Sr^* $(Sr/\sqrt{(Pr \times Nd)})_{PM}$ in five diamonds vary between no, and strong negative anomalies (Sr^*=0.03-1) and one diamond has a positive anomaly of 1.7. Zr/Eu_{PM} range between 0.02 to 2.1.

We note that the measured Rb, Th, Zr (and Hf) and Ti values are almost invariably between LOQ and LOD (Figure 5a,b; Table 1). However, relative to elements of similar compatibility, concentrations are consistent to other microinclusion-bearing diamonds measured in previous studies [e.g. 22, 23, 26, 27]. The HREE Tm, Yb and Lu are between LOQ and LOD for diamond 508, where absolute HREE contents are low (Figure 5a), and for diamond 509A, from which only 0.1 mg of ablated material was collected (Figure 5b; Table 1). In these two cases, the levels of these elements and their PM normalized patterns show no difference compared to the other diamonds or duplicates of the same diamond that were analyzed in the present study. The similarity in HREE content and pattern for duplicate analyses of the same diamond (509A-D) is also recorded for most trace elements. Moderate to large variations appear only for some of the most incompatible elements (i.e. Cs, Rb, Th, U and Nb; Figure 5b).

Our trace element data exhibit PM normalized patterns that are highly similar in shape to those of previously analyzed microinclusion-bearing diamonds [22, 23, 26]. Comparison between the patterns of diamond 509 using the new sampling technique and on-line LA-ICPMS confirm the accuracy of the analysis results of both methods (Fig. S1). Specifically compared to published off-line ablation analyses, the data in the present off-line ablation study are within the range but mostly at the lower abundance levels (except for diamond 509; Fig. 5). Variation in abundance levels is mostly a direct result of the number of microinclusions in a diamond, and the low levels in the studied diamond are in agreement with the diamond's translucent appearance, which indicates a relatively low density of microinclusions (excluding diamond 509, which is opaque). Nonetheless, our new ablation technique allows enough material for quantitative analysis of all REEs including the most compatible ones, which were usually below the LOQ of previous ablation methods (i.e. Ho to Lu; Figure 5a) [22, 23, 26].

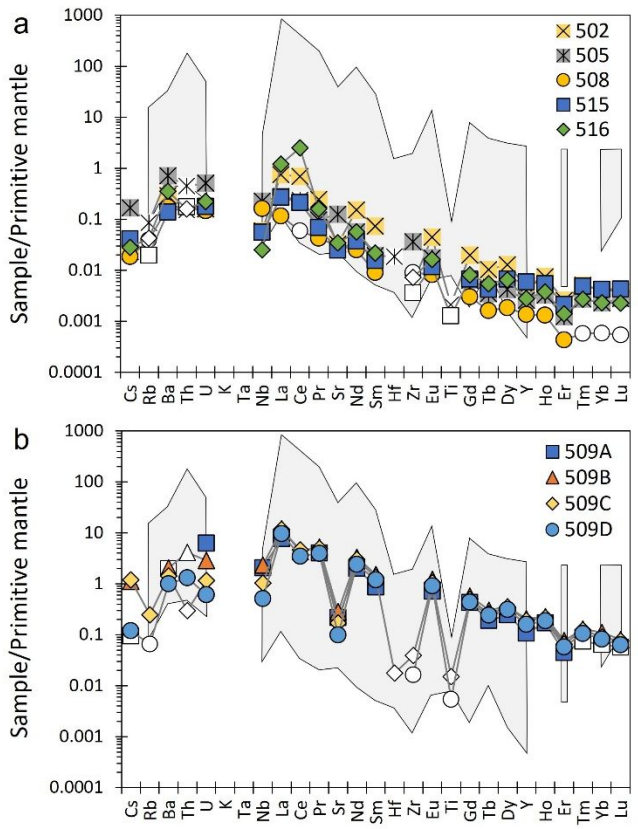

Fig. 5 Primitive mantle normalized trace element patterns in the studied diamonds; **(a)** diamonds 502, 505, 508, 515 and 516, **(b)** four duplicates of diamond 509. White filled symbols are data falling between LOQ and LOD (between 10×σ and 3×σ of the TPB), and are regarded as qualitative. The trace element concentrations normalized to the weights of the ablated material of each diamond sample are presented in Table 2. For comparison, the shaded area represents the range in 40 microinclusion-bearing diamonds from Africa, Canada and Siberia that were measured using previous off-line laser ablations and analyses methods [26, 27]. Primitive-mantle values are from [53].

Sr-Nd-Pb isotope compositions

The amount of Sr in the four duplicates of diamond 509 vary between 0.96-12.15 ng and the TPB constitutes between 3-39% of the analyzed samples (Fig. 6; Table 2). Nd varies between 0.30-15.95 ng and the TPB constitutes between 0.04-2.12%, respectively. The contribution of the TPB in the case of Pb is higher; the amount of Pb varies between 0.56-3.15 ng and the TPB constitutes between 7-41% of the analyzed samples. These variations are reflected in the isotopic composition determined for the different duplicates (mostly of Sr and Pb): $^{87}Sr/^{86}Sr$ ratio range between 0.70667 ± 6 and 0.70573 ± 2; $^{143}Nd/^{144}Nd$ between 0.511908 ± 106 and 0.511914 ± 15; and Pb isotope compositions between $^{206}Pb/^{204}Pb$=18.346 ± 6 to 17.617 ± 3, $^{207}Pb/^{204}Pb$=15.614 ± 6 to 15.519 ± 3 and $^{208}Pb/^{204}Pb$=38.088 ± 17 to 37.569 ± 98.

Figure 6 shows a strong correlation between the Sr isotope ratios, analyte amounts and the corresponding blank levels. Such a relationship allows a simple blank correction when the isotopic composition of the blank is known. The isotopic compositions of the individual TPB were too small to be precisely determined in this study. The data indicate, however, that the two large duplicates of 10-12 ng Sr (509C,D) closely represent the Sr isotope ratio of the ablated diamond (0.70573-0.70580 ± 3; Table 2). In contrast, measuring 2 ng or less of Sr leads to higher Sr isotope values that deviate by about 0.5-2‰ (i.e. 509A,B). Such variations, in the 3rd decimal place for Sr isotope ratios are significant when considering mantle-derived samples. For example, the complete mantle array as sampled by basalts vary between $^{87}Sr/^{86}Sr$=0.702 to $^{87}Sr/^{86}Sr$=0.707 [54, 55]. A precise blank correction is therefore required in future studies.

In the case of Nd isotope ratios, the impact of the blank is unresolvable. The two large duplicate samples contain ~15 ng Nd (509C,D) and yield identical results (0.511913-0.511914 ± 15; Table 2), representing the isotopic ratio of the ablated diamond. The smaller duplicates of ~1 ng and 300 pg (509A,B) also have indistinguishable isotopic results but with larger errors (Fig. 6).

The results for Pb isotope compositions are less straightforward. The two large duplicates although differing in Pb amount by a factor of two, 3.1 ng in 509C and 1.4 ng in 509D, yielded indistinguishable $^{206}Pb/^{204}Pb$, $^{207}Pb/^{204}Pb$ and $^{208}Pb/^{204}Pb$ ratios (Fig. 6; Table 2). This is consistent with the comparable Sr and Nd isotope compositions of these two duplicates, suggesting that their Pb isotopes ratios reflect the composition of the ablated diamond. In contrast, the two smaller duplicates (509A,B) have more radiogenic Pb isotope compositions, which we attribute to blank contribution. This is consistent with the blank contribution of radiogenic Sr in these two duplicates; although we note that variation for the amount of analyte and blank does not correlate between Sr and Pb (Fig. 6). A possible explanation for this discrepancy is that more than one source contributed to the Pb blank in the present study with varying amounts from pre-ablation sample preparation and post-ablation processing (but not during chromatographic separation that contributed only 1 pg of Pb).

A note about compositional homogeneity of individual diamonds

To date, only a handful of microinclusion-bearing diamonds were reported that record a significant major element chemical zoning and/or radial core-to-rim variation of HDF composition [11, 56-58]. All others, >95% of ~300 microinclusion-bearing diamonds analyzed for major element HDF composition have limited (less than 20% relative) and random variation with no clear core-to-rim evolution. Similar results are recorded in the diamonds analyzed in the present study (Fig. 2).

Laser ablation ICPMS analyses determine the average trace element composition of thousands to millions of microinclusions in the ablated volume of the diamond. Multiple ablation analyses of different parts of an individual homogeneous diamond agree to better than 15% [11, 19, 21-23, 26]. The duplicate analyses of diamond 509 in the present study show similar results, especially for REE contents (Fig. 5). Other elements show larger variation that we attribute mainly to their relatively high content in the TPB of the present study. Nonetheless, the collective data show that diamonds with

homogeneous HDF composition are also homogenous for trace elements.

The case for isotopic composition is more ambiguous. Klein-BenDavid et al. (2010) [27] reported repeated Sr isotope analysis in six diamonds that are homogeneous for their major element composition. Four of these diamonds recorded significant Sr isotope variation in the third decimal place (between 1-8‰), while the other two show a variation of 0.1‰ and 0.01‰. These data suggested that HDF microinclusions can be heterogenous for their isotopic composition over the area of individual diamond growth. We note, however, that the weight of the ablated material in all those duplicates is low and varies between 0.04-0.27 mg (Klein-BenDavid, personal communication). Figure 6 indicates that such small ablations may be influenced by significant blank contribution. The present study thus provides an alternative explanation for the isotopic variations reported by Klein-BenDavid et al. (2010) [27]; they may result from insufficient amount of analyte. Although pending additional data, this suggestion is consistent with indistinguishable Nd isotope ratios of all duplicates of diamond 509 (Fig. 6), as well as the relatively constrained variation of Nd isotope ratios reported by Klein-BenDavid et al. (2010) [27] for the diamonds that show large $^{87}Sr/^{86}Sr$ isotope variation.

Conclusions

We present a new laser ablation technique using a powerful laser that allows ablation of a few mg of a diamond; significantly more efficiently compared to previous studies. The ablation is performed in a chemical clean environment while the diamond is submerged in milli-Q water, allowing simple retrieval of the nanosized analyte particles for following chemical processing and analyses.

Improving the amount and yield of the ablated material is a key issue that facilitates the chemical measurements of microinclusion-bearing diamonds. The new ablation technique provides enough material for quantitative analysis of all rare-earth elements (REEs), even in diamonds of low element abundance levels. Utilizing TIMS with 10^{11} and 10^{13} resistors ensures successful Sr, Nd, and Pb isotope analyses also for small ablations of <1 mg. In this initial setup, however, the blank contribution can impact Sr and Pb isotope compositions that result in substantially more radiogenic values. Diamond ablations of a few mg provide sufficient analyte to yield reproducible Sr-Nd-Pb isotope ratios that reflect the composition of the ablated diamond.

The present study results suggest that individual diamonds carrying homogeneous HDFs (as reflected in EPMA analyses of the major elements of individual microinclusions) are also homogeneous for trace element and isotopic compositions.

The new technique and the process of diamond ablation will be improved using a motorized stage. In addition, optimizing the cleaning and sample handling and processing methods, before and after ablation takes place, will deliver lower blank levels. Such improvements are expected to be beneficial for the determination of many trace elements in gem-quality diamonds that are barren of visible microinclusions and hard to analyze. Moreover, together with the TIMS analyses using 10^{13} resistors, the new ablation technique may provide the means for radiogenic isotopic analyses of such diamonds.

Author Contributions

Y.W. conceived and developed the project, and wrote the paper. Y.W. and S.J. developed the diamond-in-water ablation, established the technique, and performed the ablations at CU. Y.W. performed the trace element analyses together with L.B. at LDEO, and chromatography and Isotopic analysis together with J.M.K and O.E. at VU. J.M.K. and G.R.D. contributed intellectually to the paper.

Conflicts of interest

There are no conflicts to declare.

Acknowledgements

We thank E. Ponzevera for help with the first experimental ablations of diamond-in-water, R. Harris for his help with manufacturing the ablation cell, L. Bolge for help with trace elements analyses, and M. Schrauder for the donation of diamonds used in this study. Y.W. acknowledges support by ISF Grant No. 2015/18, NSF Grant EAR-1348045 and Europlanet 2020 RI Grant 18-EPN5-002. Europlanet 2020 RI has received funding from the European Union's Horizon 2020 research and innovation programme under grant agreement No 654208.

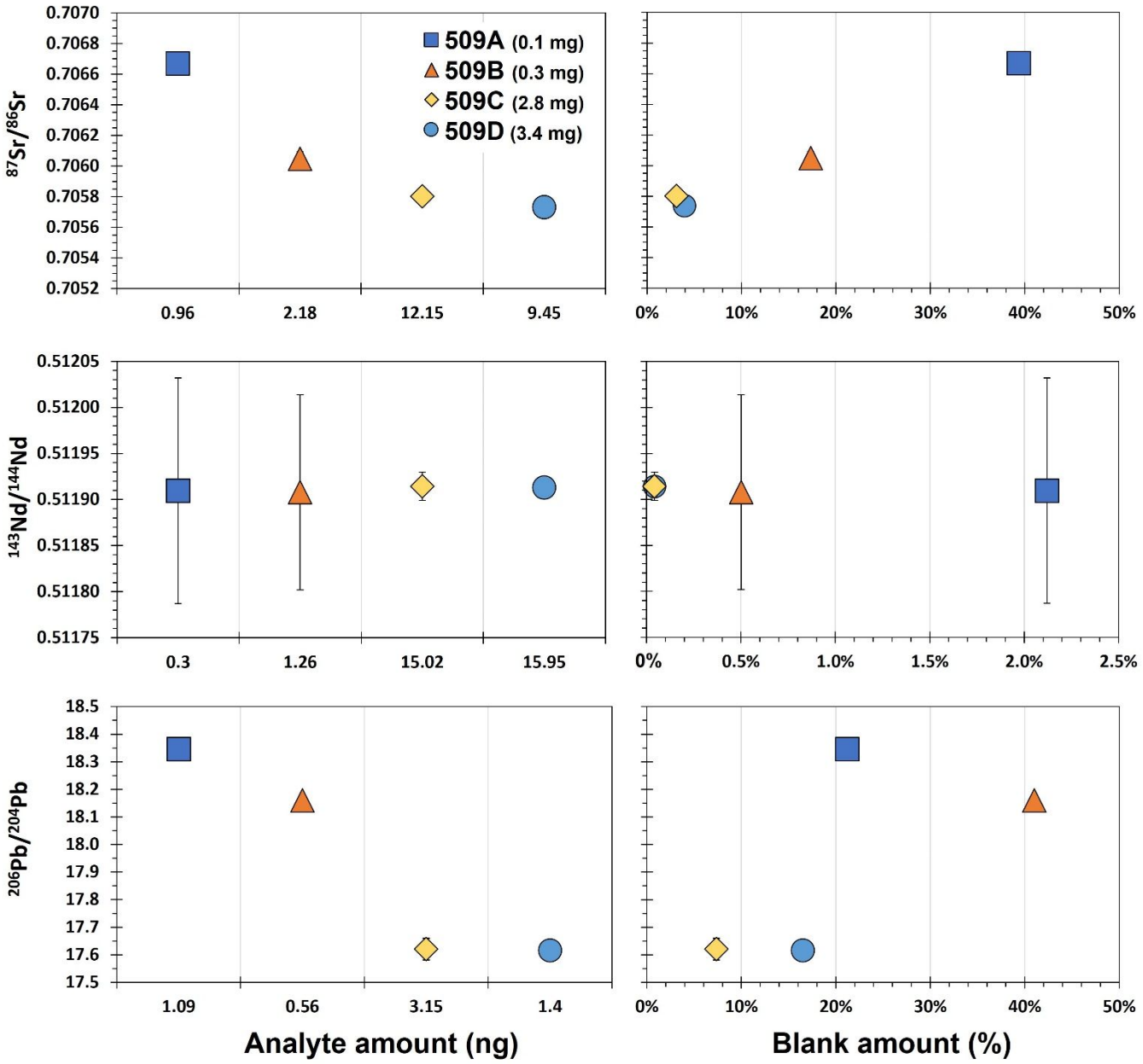

Fig. 6 Sr, Nd and Pb isotope ratios of 4 duplicates (A-D) of diamond 509 produced by ablation of 0.1, 0.3, 2.8 and 3.4 mg. The isotopic compositions of the different duplicates are presented against the analyte amount (in ng) as determined by TIMS measurements (left panels), and against the total procedural blank amount (in %) relative to the analyzed sample (right panels). Error bars represent ± 2σ and are smaller than the size of the symbols for the majority of data points.

Table 1 Trace elements compositions of the analyzed diamonds

Diamond	502	505	508	509 A	509 B	509 C	509 D	515	516	LOQ
Ablation time (min)	60	60	60	1	5	30	30	60	60	
Ablated material (mg)	11.2	4.9	9.5	0.1	0.3	2.8	3.4	14.4	9.7	
Element (ppb)[a]										
Cs	0.48	3.5	0.39	*[c]2.0*	23.5	25.2	2.5	0.86	0.59	[b]0.0004
Rb		*51.4*	*23.3*			148	*39.1*	*11.7*	*25.4*	0.41
Ba	1912	4698	1131	*13066*	13468	9404	6573	916	2333	2.6
Th	*12.1*	*35.5*	*13.9*		*332*	*23.8*	105	*13.9*	*12.6*	0.21
U	3.2	10.3	3.0	128	58.5	23.5	12.4	3.6	4.5	0.0055
Nb	39.1	148	106	1362	1528	683	338	36.7	16.6	0.11
La	486	180	74.5	4998	7798	7532	6291	175	774	0.36
Ce	1150	*394*	*99.1*		*7144*	7735	5834	355	4168	2.8
Pr	62.4	24.8	10.8	1016	1345	1254	1006	17.4	40.2	0.0051
Sr	643	2486	605	4336	5621	3393	1959	489	686	0.26
Nd	189	70.6	31.4	2527	4145	3787	3006	46.9	70.6	0.013
Sm	29.4	7.9	3.7	351	617	538	484	6.3	8.8	0.0048
Hf		*5.3*				*5.0*				0.044
Zr	*58.7*	382	*95.6*			*411*	*172*	*37.8*	*75.5*	1.3
Eu	6.8	2.7	1.3	110	186	163	140	1.8	2.5	0.0006
Ti	*2548*					*18137*	*6539*	*1539*		60.7
Gd	10.7	3.5	1.6	233	313	271	237	3.6	4.4	0.0015
Tb	1.0	0.34	0.16	19.0	30.2	25.8	24.0	0.41	0.54	0.0002
Dy	8.6	2.8	1.2	166	241	236	210	4.5	4.4	0.0030
Y	21.0	11.1	5.8	464	882	821	693	25.2	12.0	0.013
Ho	1.1	0.48	0.19	25.5	33.9	32.1	27.9	0.81	0.56	0.0004
Er	1.1	0.54	0.19	19.5	33.7	28.5	25.2	0.93	0.61	0.0007
Tm	0.34	0.18	*0.04*	*5.0*	8.8	8.5	7.2	0.33	0.18	0.0006
Yb	1.8	1.0	*0.26*	*28.5*	48.6	39.7	36.1	1.9	1.0	0.0040
Lu	0.26	0.19	*0.04*	*3.8*	5.4	5.1	4.3	0.29	0.15	0.0005

[a]Concentrations (in PPB) are corrected for the average total procedural blank values and normalized to the weight of the ablated material.
[b]limit of quantification (LOQ) in ppb is calculated as 10 times the uncertainty on the blank/background, i.e. LOQ=10×$\sigma_{(\text{total procedural blank-TPB})}$.
[c]Values in red italics are between the limit of quantification (LOQ) and the limit of detection (LOD), where LOQ=10×$\sigma_{(\text{TPB})}$ and LOD=3×$\sigma_{(\text{TPB})}$.
Value below the minimum detection limit are not shown.

Table 2 Sr-Nd-Pb isotope compositions of diamond 509 duplicate samples

Diamond	509 A	509 B	509 C	509 D	TPB A	TPB B
Sr (ng)[a]	0.96	2.18	12.15	9.45	373 (pg)[b]	382
TPB%[c]	39%	17%	3%	4%		
$^{87}Sr/^{86}Sr$	0.70667 (6)	0.70605 (5)	0.70580 (3)	0.70573 (2)		
Nd (ng)	0.30	1.26	15.02	15.95	4.8	7.9
TPB%	2.12%	0.50%	0.04%	0.04%		
$^{143}Nd/^{144}Nd$	0.511910 (123)	0.511908 (106)	0.511914 (15)	0.511913 (11)		
Pb (ng)	1.09	0.56	3.15	1.40	225	239
TPB%	21%	41%	7%	17%		
$^{206}Pb/^{204}Pb$	18.346 (6)	18.160 (6)	17.620 (39)	17.617 (3)		
$^{207}Pb/^{204}Pb$	15.614 (6)	15.598 (5)	15.531 (33)	15.519 (3)		
$^{208}Pb/^{204}Pb$	38.088 (17)	38.024 (13)	37.569 (98)	37.638 (8)		

[a]The amount of Sr (in ng) in the analyzed samples normalized to the weight of the ablated material of each diamond - $Sr_{(\text{analyzed sample})}$. The same is applicable for Nd and Pb.
[b]The amount of Sr in total procedural blanks (TPB; in pg) - $Sr_{(\text{TPB})}$. The same is applicable for Nd, Sm and Pb.
[c]Percent of TPB = $Sr_{(\text{average TPB})}/Sr_{(\text{analyzed sample})}$. The same is applicable for the amount of Nd, Sm and Pb.

References

1. E. M. Smith, M. G. Kopylova, G. M. Nowell, D. G. Pearson and J. Ryder, *Geology*, 2012, **40**, 1071-1074.
2. S. Timmerman, H. Yeow, M. Honda, D. Howell, A. L. Jaques, M. Y. Krebs, S. Woodland, D. G. Pearson, J. N. Ávila and T. R. Ireland, *Chemical Geology*, 2019, **515**, 22-36.
3. Y. Kempe, Y. Weiss, I. Chinn and O. Navon, *Lithos*, 2021, 106285.
4. Y. Weiss, Y. Kiro, C. Class, G. Winckler, J. W. Harris and S. L. Goldstein, *Nature Communications*, 2021, **12**, 2667.
5. M. Schrauder, C. Koeberl and O. Navon, *Geochimica Et Cosmochimica Acta*, 1996, **60**, 4711-4724.
6. D. A. Zedgenizov, S. Y. Skuzovatov, W. L. Griffin, B. S. Pomazansky, A. L. Ragozin and V. V. Kalinina, *Contributions to Mineralogy and Petrology*, 2020, **175**, 106.
7. Y. Weiss, W. L. Griffin, S. Elhlou and O. Navon, *Chemical Geology*, 2008, **252**, 158-168.
8. O. Navon, I. D. Hutcheon, G. R. Rossman and G. J. Wasserburg, *Nature*, 1988, **335**, 784.
9. M. Schrauder and O. Navon, *Geochimica et Cosmochimica Acta*, 1994, **58**, 761-771.
10. E. S. Izraeli, J. W. Harris and O. Navon, *Earth and Planetary Science Letters*, 2001, **187**, 323-332.
11. Y. Weiss, R. Kessel, W. L. Griffin, I. Kiflawi, O. Klein-BenDavid, D. R. Bell, J. W. Harris and O. Navon, *Lithos*, 2009, **112**, 660-674.
12. O. Klein-BenDavid, A. M. Logvinova, M. Schrauder, Z. V. Spetius, Y. Weiss, E. H. Hauri, F. V. Kaminsky, N. V. Sobolev and O. Navon, *Lithos*, 2009, **112, Supplement 2**, 648-659.
13. E. L. Tomlinson, A. P. Jones and J. W. Harris, *Earth and Planetary Science Letters*, 2006, **250**, 581-595.
14. S. Timmerman, A. L. Jaques, Y. Weiss and J. W. Harris, *Chemical Geology*, 2018, **483**, 31-46.
15. D. A. Zedgenizov, A. L. Ragozin, V. S. Shatsky, D. Araujo, W. L. Griffin and H. Kagi, *Lithos*, 2009, **112, Supplement 2**, 638-647.
16. D. M. Bibby, *Geochim. cosmochim. Acta*, 1979, **43**, 415-423.
17. T. Akagi and A. Masuda, *Nature*, 1988, **336**, 665-667.
18. S. Rege, S. Jackson, W. L. Griffin, R. M. Davies, N. J. Pearson and S. Y. O'Reilly, *Journal of Analytical Atomic Spectrometry*, 2005, **20**, 601-611.
19. S. Rege, W. L. Griffin, N. J. Pearson, D. Araujo, D. Zedgenizov and S. Y. O'Reilly, *Lithos*, 2010, **118**, 313-337.
20. D. A. Zedgenizov, A. L. Ragozin and V. S. Shatsky, *Doklady Earth Sciences*, 2007, **415**, 961-964.
21. Y. Weiss and S. L. Goldstein, *Mineralogy and Petrology*, 2018, 1-19.
22. E. L. Tomlinson, W. Müller and Eimf, *Earth and Planetary Science Letters*, 2009, **279**, 362-372.
23. Y. Weiss, W. L. Griffin and O. Navon, *Earth and Planetary Science Letters*, 2013, **376**, 110-125.
24. J. McNeill, D. Pearson, O. Klein-BenDavid, G. Nowell, C. Ottley and I. Chinn, *Journal of Physics: Condensed Matter*, 2009, **21**, 364207.
25. J. McNeill, 2011.
26. O. Klein-BenDavid, D. G. Pearson, G. M. Nowell, C. Ottley, J. C. R. McNeill, A. Logvinova and N. V. Sobolev, *Geochimica et Cosmochimica Acta*, 2014, **125**, 146-169.
27. O. Klein-BenDavid, D. G. Pearson, G. M. Nowell, C. Ottley, J. C. R. McNeill and P. Cartigny, *Earth and Planetary Science Letters*, 2010, **289**, 123-133.
28. Y. Weiss, J. McNeill, D. G. Pearson, G. M. Nowell and C. J. Ottley, *Nature*, 2015, **524**, 339-342.
29. J. M. Koornneef, I. Nikogosian, M. J. van Bergen, R. Smeets, C. Bouman and G. R. Davies, *Chemical Geology*, 2015, **397**, 14-23.
30. O. Klein-BenDavid, R. Wirth and O. Navon, *American Mineralogist*, 2006, **91**, 353-365.
31. A. M. Logvinova, R. Wirth, E. N. Fedorova and N. V. Sobolev, *European Journal of Mineralogy*, 2008, **20**, 317-331.
32. A. Logvinova, D. Zedgenizov and R. Wirth, *Minerals*, 2019, **9**, 50.
33. B. M. Jablon and O. Navon, *Earth and Planetary Science Letters*, 2016, **443**, 41-47.
34. M. Y. Krebs, D. G. Pearson, T. Stachel, F. Laiginhas, S. Woodland, I. Chinn and J. Kong, *Lithos*, 2019, **324-325**, 356-370.
35. S. Barcikowski, *The Journal of Physical Chemistry C*, 2011, **115**, 4985-4985.
36. A. V. Kabashin and M. Meunier, *Journal of Applied Physics*, 2003, **94**, 7941-7943.
37. E. Hywel Evans, C. D. Palmer and C. M. M. Smith, *Journal of Analytical Atomic Spectrometry*, 2012, **27**, 909-927.
38. P. Liu, H. Cui, C. X. Wang and G. W. Yang, *Physical Chemistry Chemical Physics*, 2010, **12**, 3942-3952.
39. E. A. Ganash, G. A. Al-Jabarti and R. M. Altuwirqi, *Materials Research Express*, 2019, **7**, 015002.
40. D. N. Douglas, J. L. Crisp, H. J. Reid and B. L. Sharp, *Journal of Analytical Atomic Spectrometry*, 2011, **26**, 1294-1301.
41. S. Okabayashi, T. D. Yokoyama, Y. Kon, S. Yamamoto, T. Yokoyama and T. Hirata, *Journal of Analytical Atomic Spectrometry*, 2011, **26**, 1393-1400.
42. Y. Iida, A. Tsuge, Y. Uwamino, H. Morikawa and T. Ishizuka, *Journal of Analytical Atomic Spectrometry*, 1991, **6**, 541-544.
43. J. M. Koornneef, M. U. Gress, I. L. Chinn, H. A. Jelsma, J. W. Harris and G. R. Davies, *Nature Communications*, 2017, **8**, 648.
44. J. M. Koornneef, I. Nikogosian, M. J. van Bergen, P. Z. Vroon and G. R. Davies, *Nature Communications*, 2019, **10**, 3237.
45. M. Klaver, R. J. Smeets, J. M. Koornneef, G. R. Davies and P. Z. Vroon, *Journal of Analytical Atomic Spectrometry*, 2016, **31**, 171-178.
46. J. M. Koornneef, C. Bouman, J. B. Schwieters and G. R. Davies, *Analytica Chimica Acta*, 2014, **819**, 49-55.
47. M. Thirlwall, *Chemical Geology*, 2002, **184**, 255-279.
48. D. Weis, B. Kieffer, C. Maerschalk, J. Barling, J. de Jong, G. A. Williams, D. Hanano, W. Pretorius, N. Mattielli, J. S. Scoates, A. Goolaerts, R. M. Friedman and J. B. Mahoney, *Geochemistry, Geophysics, Geosystems*, 2006, **7**.
49. L. A. Currie, *Analytical Chemistry*, 1968, **40**, 586-593.
50. S. Timmerman, M. Y. Krebs, D. G. Pearson and M. Honda, *Geochimica et Cosmochimica Acta*, 2019, **257**, 266-283.
51. S. Timmerman, M. Honda, A. D. Burnham, Y. Amelin, S. Woodland, D. G. Pearson, A. L. Jaques, C. L. Losq, V. C.

Bennett, G. P. Bulanova, C. B. Smith, J. W. Harris and E. Tohver, *Science*, 2019, **365**, 692-694.
52. G. L. Melton, J. McNeill, T. Stachel, D. G. Pearson and J. W. Harris, *Chemical Geology*, 2012, **314-317**, 1-8.
53. W. F. McDonough and S. S. Sun, *Chemical Geology*, 1995, **120**, 223-253.
54. A. Stracke, *Chemical Geology*, 2012, **330**, 274-299.
55. A. W. Hofmann, *Nature*, 1997, **385**, 219-229.
56. O. Klein-BenDavid, E. S. Izraeli, E. Hauri and O. Navon, *Lithos*, 2004, **77**, 243-253.
57. A. A. Shiryaev, E. S. Izraeli, E. H. Hauri, O. D. Zakharchenko and O. Navon, *Russian Geology and Geophysics*, 2005, **46**, 1185-1201.
58. D. A. Zedgenizov, A. L. Ragozin, V. S. Shatsky, D. Araujo and W. L. Griffin, *Russian Geology and Geophysics*, 2011, **52**, 1298-1309.